

1    **COVER PAGE**

2    **Authors:** Todd J. Zurlinden<sup>1</sup>, Garrett J. Eppers<sup>1</sup>, Brad Reisfeld<sup>1,2</sup>

3  
4    **Title:** A physiologically-based pharmacokinetic model of rifapentine and 25-desacetyl-  
5    rifapentine disposition in humans

6  
7    **Affiliation:**

8  
9    [1] Department of Chemical and Biological Engineering  
10   Colorado State University  
11   Fort Collins, CO USA 80523-1370

12  
13   [2] School of Biomedical Engineering  
14   Colorado State University  
15   Fort Collins, CO USA 80523-1301

16  
17   **Corresponding Author:**

18  
19   Brad Reisfeld  
20   Department of Chemical and Biological Engineering  
21   1370 Campus Delivery  
22   Colorado State University  
23   Fort Collins, CO USA 80523-1370  
24   Tel: 970-491-1019  
25   Fax: 970-491-7369  
26   Email: brad.reisfeld@colostate.edu

28   **Running title:** A PBPK model for rifapentine in humans

29

30 **ABSTRACT**

31 Rifapentine (RPT) is a rifamycin antimycobacterial and, as part of a combination therapy, is  
32 indicated for the treatment of pulmonary tuberculosis (TB) caused by *Mycobacterium*  
33 *tuberculosis* (MTB). Although results from a number of studies indicate that rifapentine has the  
34 potential to shorten treatment duration and enhance completion rates compared with other  
35 rifamycin agents utilized in anti-tuberculosis drug regimens (1–4), its optimal dose and exposure  
36 in humans are unknown. To help inform such an optimization, a physiologically-based  
37 pharmacokinetic (PBPK) model was developed to predict time-course, tissue-specific  
38 concentrations of RPT and its active metabolite, 25-desacetyl-rifapentine (dRPT) in humans  
39 following specified administration schedules for RPT. Starting with the development and  
40 verification of a PBPK model for rats, the model was extrapolated and then tested using human  
41 pharmacokinetic data. Testing and verification of the models included comparisons of  
42 predictions to experimental data in several rat tissues and time-course RPT and dRPT plasma  
43 concentrations in humans from several single- and repeated-dosing studies. Finally, the model  
44 was used to predict RPT concentrations in the lung during the intensive and continuation phases  
45 of a current recommended TB treatment regimen. Based on these results, it is anticipated that the  
46 PBPK model developed in this study will be useful in evaluating dosing regimens for RPT and  
47 for characterizing tissue-level doses that could be predictors of problems related to efficacy or  
48 safety.

49

Accepted Manuscript Posted Online  
Antimicrobial Agents and Chemotherapy  
AAC  
Antimicrobial Agents and Chemotherapy

50 Rifapentine (RPT) is a rifamycin-class antibiotic indicated for the treatment of pulmonary  
51 tuberculosis (TB) caused by *Mycobacterium tuberculosis* (MTB) and in the treatment of latent  
52 TB infection in patients at high risk of progression to TB disease. RPT has a longer half-life,  
53 increased affinity to serum protein binding (5), and lower minimum inhibitory concentration  
54 (MIC) against MTB than rifampin, which is currently used as part of several first-line TB  
55 treatment regimens (2, 6). Moreover, the primary metabolite for RPT, 25-desacetyl-rifapentine  
56 (dRPT), has also been found to be active against MTB, although at markedly lower mean  
57 inhibitory concentrations (5–7). Because of these characteristics, RPT has been the subject of a  
58 number of clinical pharmacology studies aimed at evaluating pharmacokinetics and developing  
59 effective therapies (1, 3, 8–16). Although data from these investigations are valuable in their own  
60 right, mathematical modeling offers a way to complement these studies, synthesize their  
61 disparate data, and provide the clinician an additional tool to characterize and predict the  
62 absorption, distribution, metabolism, and excretion (ADME) of RPT under dosing conditions of  
63 interest.

64 One of the very few such mathematical models was developed by Savic et al. (4) who used a  
65 classical compartmental modeling approach to assess human population pharmacokinetics of  
66 both RPT and dRPT. This model described the absorption, metabolism, and clearance of these  
67 two species and accurately predicted their time-course plasma concentrations in healthy  
68 volunteers. Unfortunately, compartmental concentrations in this model were not directly  
69 relatable to those in actual tissues of interest (e.g., the lung and liver) because the effects of  
70 plasma protein binding and blood-tissue partitioning of the parent drug and metabolite were not  
71 included. Moreover, because the study utilized data from healthy subjects, the effects of the  
72 disease on pharmacokinetic outcomes could not be characterized.

Accepted Manuscript Posted Online  
Antimicrobial Agents and Chemotherapy  
AAC  
Accepted Manuscript Posted Online  
Antimicrobial Agents and Chemotherapy

73 A finer-grained approach that specifically includes relevant physiological and biochemical  
74 effects and processes and facilitates examination of organ or tissue-level pharmacokinetics is  
75 physiologically-based pharmacokinetic (PBPK) modeling. Regrettably, few PBPK models have  
76 been developed for anti-TB drugs, let alone RPT. Using targeted experimental data in mice,  
77 Reisfeld et al. (17) developed a PBPK model to describe the biodistribution of the second-line  
78 TB agent, capreomycin, and because capreomycin is nephrotoxic (18), PBPK modeling allowed  
79 for tissue-specific concentration predictions at both the site of action for the antibiotic effect, the  
80 lung, and the site of potential toxicity, the kidney. Subsequently, Lyons et al. (19) used a rich set  
81 of literature data to create a PBPK model to describe the disposition of rifampin which, as noted  
82 earlier, is a first-line agent in current therapies for TB. Although the above models are useful in  
83 simulating and comparing the disposition of anti-TB drugs in tissues of interest, they were  
84 developed using data from rodents and currently have limited applicability to humans.

85 To begin to address this gap, the principal aims of this study were to (i) develop a PBPK model  
86 to predict the ADME for rifapentine and its active metabolite in humans, (ii) test the model  
87 against available human study data, and (iii) make tissue-specific predictions of concentrations  
88 of RPT and dRPT in the lung and compare those to the MIC. This latter aim is particularly  
89 relevant because current dosing recommendations for anti-TB drugs are guided by knowledge of  
90 the unbound concentration of the agent in the plasma and by comparing this free fraction to the  
91 known MIC against MTB (14). Because this plasma concentration may not accurately reflect that  
92 in the lung, the recommended dose may not provide the desired level of antibiotic effect.

### 93 MATERIALS AND METHODS

94 **Approach.** To achieve the study aims, two PBPK models were developed, parameterized, and  
95 tested: one specific to the rat (R-PBPK) and another for humans (H-PBPK). The models shared

96 the same compartmental structure and set of governing equations, with differences only in the  
97 parameter values, principally related to physiology and metabolism. Starting with development  
98 of the R-PBPK, tissue specific pharmacokinetic data were used to compute key drug-tissue  
99 properties (e.g., partition coefficients) that were later utilized in the H-PBPK. Ultimately, both  
100 the R-PBPK and H-PBPK were parameterized and verified using relevant sets of training and  
101 test data. Further details are given below.

102 **Experimental data.** Pharmacokinetic data for RPT in rats were obtained from the work of  
103 Assandri et al. (20), which provided (i) drug concentrations in the plasma under multiple dosing  
104 conditions, (ii) concentrations obtained from homogenates of several relevant tissues following  
105 oral dosing, and (iii) the fraction of drug bound to plasma proteins over time. For development of  
106 the human model, a comprehensive review of the literature was conducted to identify  
107 pharmacokinetic studies where RPT was administered to adults as either a single dose or via  
108 repeated doses. Emphasis was placed on studies in which concentrations of both parent RPT and  
109 its metabolite dRPT were quantified because these coincident data could be used in the  
110 estimation of relevant metabolism and dRPT-specific parameters. As shown in Table 2, these  
111 data were divided into two parts: a ‘training’ set used to determine unknown model parameters  
112 and a ‘validation’ set, used to test and verify the model predictions.

113 **PBPK models.** The common PBPK model structure is shown in Fig. 1. The model comprises a  
114 set of compartments for RPT, identical to those used previously for rifampin (19), integrated  
115 with a simpler structure for the metabolite, dRPT, which consisted of only the lung and a *lumped*  
116 peripheral compartment. The compartmental species mass balance equations are similar to those  
117 used in this prior study (see the Appendix) with the exception of the description of oral

118 absorption fraction for the parent compound and the explicit quantitation of the metabolite  
 119 concentration over time described below.

120 Consistent with the experimental results from Assandri *et al.* (20), oral absorption was specified  
 121 to be dose dependent. In particular, the following form was used to describe the oral fraction  
 122 absorbed,  $F_a$ :

$$123 \quad F_a = \frac{F_{a,k}}{D + F_{a,k}},$$

124 where  $D$  is the oral dose and  $F_{a,k}$  represents a constant to be fit from the data.

125 Because the metabolite dRPT is active against MTB and its level has been measured in several  
 126 studies in humans, the present model included equations to explicitly track its rate of formation  
 127 and distribution over time. The deacetylation reaction to transform RPT to dRPT in the liver for  
 128 humans was assumed to follow Michaelis-Menten kinetics (21),

$$129 \quad v = \frac{V_M C_{liver}^{RPT}}{K_M + C_{liver}^{RPT} + \frac{(C_{liver}^{RPT})^2}{K_I}},$$

130 where  $v$  is the rate of RPT deacetylation,  $V_M$ ,  $K_M$ , and  $K_I$  represent the maximum reaction rate,  
 131 the Michaelis-Menten constant, and the substrate inhibition constant for RPT deacetylation,  
 132 respectively. While its mechanism of action is currently unknown, *in vitro* studies have  
 133 demonstrated the activity of dRPT against MTB (7), and because this species may exhibit similar  
 134 antibiotic effects *in vivo*, its disposition may be of interest when characterizing anti-TB therapies  
 135 involving RPT. Interestingly, although the levels of dRPT are quantifiable in humans following  
 136 RPT administration (3, 8–12, 14–16), similar studies in rats have shown that this chemical is

137 undetectable in the plasma (20). Consistent with this observation, the metabolic transformation  
138 of RPT to dRPT was not included in the R-PBPK.

139 Lastly, rather than using *in vitro* results for RPT and dRPT protein binding, unbound fractions  
140 for this PBPK model were calculated using results from TB infected patients following RPT  
141 dosing (22).

142 **Parameter estimation.** Parameters in the governing PBPK model equations were taken from the  
143 literature or were estimated using the procedures described below.

144 Physiological parameters: Physiological compartment volumes and blood flow rates for human  
145 and rat were obtained from Brown et al. (23). Compartment volumes were scaled linearly with  
146 body weight, blood flow rates were scaled with body weight to the 0.75 power (24), and the  
147 coefficient of variation for each organ volume and arterial blood flow rate was set at 0.2 and 0.3,  
148 respectively (19, 25). The resulting physiological parameters for each compartment are  
149 summarized in Table 1.

150 Partition coefficients: With data for the free concentration of RPT in the plasma (20), mean  
151 values for the tissue:blood partition coefficient,  $P_{T:blood}$ , were determined using the following  
152 equation:

$$153 P_{T:blood} = \frac{1}{BP} \left( \frac{C_{tissue}^{RPT}}{C_{plasma,f}^{RPT}} \right),$$

154 where  $BP$  is the blood:plasma partition coefficient, and  $C_{tissue}^{RPT}$  and  $C_{plasma,f}^{RPT}$  are the measured  
155 tissue and free plasma concentration of RPT, respectively. Tissue:plasma partition coefficients  
156 were computed for all model compartments based on time-course tissue concentration data (20)

157 using points during the elimination phase at which equilibrium had been reached in drug  
158 concentration between the tissue and the venous blood.

159 **Other model parameters:** To include the effect of data uncertainty and inter-study variability on  
160 model outputs, unknown parameters were estimated within a Bayesian hierarchical context (26–  
161 28). Within this context, parameters were estimated by first computing partition coefficients and  
162 other relevant parameters for the R-PBPK and then using these parameter distributions as  
163 ‘priors’ in the estimation of the human-specific parameters.

164 **Simulation methodology and computing platform.** Once the parameter distributions had been  
165 computed, a Monte Carlo approach was used to generate a large family of simulation results that  
166 would account for inter-study variability and data uncertainty. These results were then  
167 aggregated and processed to yield mean and 95% prediction intervals for pharmacokinetic  
168 outcomes of interest.

169 Data from the literature were digitized using DigitizeIt v.1.5.8 (29). Simulations of the PBPK  
170 governing equations, including the Bayesian Markov chain Monte Carlo and resulting model  
171 evaluation were conducted in MCSim v5.4 (30). Processing, analysis, and visualization of data  
172 were carried out using scripts written in Python v2.7.2 (31) utilizing the numpy (32), scipy (33),  
173 and matplotlib (34) packages. All computations were performed on a compute cluster running  
174 the 64 bit CentOS Linux operating system on six gigabit-linked Dell 2950 servers, each  
175 containing two quad-core 2.5 GHz Xeon processors and 64 GB of RAM.

**176 RESULTS**

177 Model parameter values: Using the procedures and data detailed above, distributions for  
178 unknown model parameters were estimated. The resulting parameters (posterior distributions) for  
179 both rat- and human-specific models are listed in Table 3.

180 Testing and verification of the rat-specific model. (R-PBPK): Using the computed parameters for  
181 the R-PBPK, simulations were conducted and compared to *in vivo* time-course concentration  
182 values from a literature study (20) that detailed plasma and tissue pharmacokinetics following a  
183 single 10 mg/kg oral dose in the rat. This comparison is illustrated in Fig. 2, which shows  
184 experimental data (points) and predicted mean (solid line) and 95% prediction intervals (dashed  
185 lines) for the PBPK model.

186 Testing and verification of the human-specific model (H-PBPK) for single dosing scenarios:  
187 Throughout the studies, training set data were used for parameter estimation (model calibration)  
188 while verification data were used for model evaluation (27). Using the set of parameters listed in  
189 Tables 1 and 3, simulations were run for 600, 900, and 1200 mg single oral doses of RPT and  
190 compared to the corresponding dose training and verification data referenced in Table 2. Fig. 3  
191 shows the results of these comparisons for both RPT and dRPT in the plasma over multiple  
192 studies. The range of the experimental doses shown in this figure match those in a standard  
193 treatment regimen for TB treatment (5, 35). These comparisons show that the experimental data  
194 fall within the 95% prediction intervals, indicating that the model can accurately predict the  
195 pharmacokinetics of the drug and account for the variance in this measure across the population  
196 sampled.

197 As an additional verification, pharmacokinetic measures for RPT (e.g., maximum concentration,  
198 area under the curve, and half-life) were computed from the model and compared to those from

199 the literature. In particular, Table 4 shows the predicted values from simulations of time-course  
200 plasma concentrations and those in Langdon et al. (12), which were based on experimental data  
201 that were not used in the model parameterization.

202 Testing and verification of the human-specific model (H-PBPK) for repeated dosing scenarios:  
203 Relevant to standard treatments regimens for MTB (36, 37), model simulations were conducted  
204 for three repeated dosing scenarios for which well-controlled experimental data were available:  
205 regimen A - a 600 mg dose every day starting three days after an initial 600 mg dose (10);  
206 regimen B - a 900 mg dose every two days (16); and regimen C - a 600 mg dose every three days  
207 (10). Both the experimental data and corresponding simulation results are displayed in Fig. 4.

208 Prediction of lung concentrations using the human-specific model: Along with the predicted  
209 plasma concentrations shown in Fig. 4, simulations yielded the levels of RPT and dRPT in the  
210 lung over time. As an illustration of potential antibiotic effect, Fig. 5 shows the predicted levels  
211 of RPT, dRPT, and total rifamycin over time in the lung for the three RPT oral dosing scenarios  
212 described above.

213 There are a number of current and anticipated guidelines for the treatment of both active TB  
214 disease and latent TB infection involving rifapentine as part of a combination therapy (6, 38–41).  
215 Across these regimens, doses of RPT range from 600 to 1200 mg with administration  
216 frequencies extending from daily to once weekly. To determine the pharmacokinetics and  
217 potential antibiotic effect of RPT and dRPT across these regimens, the model was used to predict  
218 lung concentrations of these species in a simulated population resulting from various doses of  
219 RPT at three administration frequencies: once weekly, twice weekly, and daily. The simulated  
220 population in these cases was the group of (virtual) individuals whose pharmacokinetics were  
221 predicted by Monte Carlo sampling across the estimated physiological and biochemical

222 parameter distributions determined using the Bayesian procedure described earlier. Fig. 6 depicts  
223 a cumulative distribution function of the dose response that indicates the probability that RPT or  
224 dRPT concentrations in the lung are above their respective MICs, which were 0.063 mg/L for  
225 RPT and 0.25 mg/L for dRPT (7).

226 **DISCUSSION**

227 Methodology: The PBPK models detailed herein utilized a system of biologically-based  
228 physiological and biochemical descriptions and species mass balance equations to make tissue-  
229 specific pharmacokinetic predictions for RPT and its metabolite, dRPT, in relevant tissue  
230 compartments for both rats and humans. The values of unknown parameters in the model system  
231 were estimated within a hierarchical Bayesian framework to incorporate data uncertainties and  
232 inter-study variability, and Monte Carlo simulations were conducted using these distributions to  
233 quantify their effect on pharmacokinetic predictions.

234 Testing and verification: Model predictions were generally in good agreement with data from the  
235 literature. As shown in Fig. 2, the experimental data corresponding to plasma and tissue (lung,  
236 kidney, and spleen) concentrations were within the 95% prediction intervals for the rat-specific  
237 PBPK model, demonstrating its ability to reasonably predict tissue-level RPT pharmacokinetics  
238 in this species. For the human-specific PBPK model, single-dose data from multiple studies for  
239 both RPT and dRPT concentrations were in reasonable concordance with results from  
240 simulations (Fig. 3). The relatively poorer agreement between predictions and data for dRPT is  
241 likely related to variability in metabolism between subjects, differences in analytical quantitation  
242 methods between studies, and/or an inadequate specification for RPT metabolism in the model.  
243 For repeated oral dosing, model predictions for RPT concentrations compare well with  
244 experimental data for all three dosing scenarios (Fig. 4). Finally, as shown in Table 4, there was

245 reasonable to very good agreement between pharmacokinetic measures, such as  $C_{\max}$  and  $AUC$ ,  
246 computed from simulations and experimental data.

247 Model predictions: A principal benefit to the PBPK approach is the ability to estimate internal  
248 doses that are generally not available in human subjects or patients. Fig. 5 shows the predicted  
249 levels of RPT, dRPT, and total rifamycin over time in the lung for three repeated oral dosing  
250 scenarios for RPT. It should be noted that dRPT does not bind to plasma protein as readily as  
251 RPT. This decrease in fractional protein binding increases the bioavailability of dRPT and results  
252 in a higher predicted concentration of metabolite within the lungs. It is also notable that for all  
253 three dosing regimens, the predicted minimum concentrations for both RPT and dRPT in the  
254 lung are significantly above their *in vitro* MICs for MTB of 0.063  $\mu\text{g}/\text{ml}$  and 0.25  $\mu\text{g}/\text{ml}$ ,  
255 respectively (7). Finally, the total rifamycin concentration is presented in this figure as an  
256 indication that there may be additional bactericidal effect owing to the presence of dRPT;  
257 however, because the mechanism of action of dRPT is not currently known, the overall  
258 pharmacodynamic effect cannot be assumed to be additive.

259 Finally, the model was used to assess the potential efficacy of regimens spanning current  
260 recommended anti-TB therapies that include RPT (35, 38–41). This assessment was conducted  
261 by computing lung-tissue concentrations and comparing those to the MIC for MTB. These  
262 results are depicted in Fig. 6, which shows the probability of the minimum steady-state drug  
263 concentration in the lungs exceeding the MIC for MTB for three distinct administration  
264 frequencies. For illustration, this figure also contains an example probability threshold of 0.98  
265 from which a *minimum protective dose* (MPD) can be found. Using this probability threshold,  
266 the MPD was seen to be 26 mg for once daily dosing, 225 mg for the twice weekly regimen, and  
267 910 mg for the once weekly administration (see Fig. 6.). Based on these estimates, anti-TB

268 regimens that include daily administration of 1200 mg RPT (39) for active TB disease exceed the  
269 predicted MPD, while those that reduce this dose and frequency for the treatment of latent TB  
270 infection to 750 mg once weekly (40), fall below the predicted MPD. It is important to note that  
271 these results do not include the antimicrobial effects of other anti-TB drugs given as part of the  
272 regimen; however, depending on the margin of safety, they could suggest possible adjustments to  
273 the dosing schedule.

274 Novel features and advantages of the present model: Unlike previous PBPK models for anti-TB  
275 drugs (17, 19), the present model was developed to make predictions of pharmacokinetics in  
276 humans. To quantify and illustrate uncertainty in simulation outputs, model development and  
277 testing included a Bayesian approach to parameter estimation and Monte Carlo simulations.  
278 These features allowed the verified model to be used to assess a current treatment regimen by  
279 comparing lung-specific predictions of antibiotic concentrations with the MIC for MTB. In  
280 addition, because administration of certain rifamycins (including rifapentine) has resulted in  
281 signs of drug induced liver injury (42), liver-specific predictions of drug levels could help inform  
282 treatments that minimize the potential for hepatotoxicity. Like most PBPK models, the one  
283 described herein allowed prediction of species concentrations in tissues/organs of interest and  
284 provided a systematic way to extrapolate across doses and between species. With these features,  
285 the model has the potential to aid in dose optimization and in the determination of how  
286 pharmacokinetic endpoints depend on alterations to anatomical, physiological, and biochemical  
287 parameters.

288 Limitations and deficiencies of the present model: The current H-PBPK currently suffers from  
289 several limitations and deficiencies: (i) it is not immediately applicable to the analysis of  
290 combination drug therapies, (ii) the pharmacokinetic predictions, while expected to be valid and

useful for a population or subpopulation, may contain too much uncertainty for individualized applications like personalized medicine, (iii) parameters for the R-PBPK were estimated using relatively few data points and inaccuracies in some of these parameters were propagated to the human-specific model, and (iv) the specification used for RPT metabolism is biologically plausible, but owing to a lack of data, has not been adequately verified.

Future directions: Using the present model as a foundation, efforts are underway to add additional anti-TB agents (e.g., isoniazid or bedaquiline) to simulate combination therapies and quantify pharmacokinetic drug-drug interactions. Other enhancements include integration of pharmacodynamic descriptions that include MTB growth and drug-induced killing kinetics (43, 44), and descriptions of RPT-induced hepatotoxicity (1, 42)

301

## 302 APPENDIX

303 The following are the governing equations for the PBPK model, which mathematically specify  
 304 the species mass balances and relevant biological phenomena in each compartment. In these  
 305 equations, the superscript,  $i$ , corresponds to either parent RPT or the dRPT metabolite. While  
 306 RPT disposition is described in all of the discrete tissue compartments, dRPT is modeled within  
 307 only two compartments: lung and peripheral. Individual tissue blood flow rates,  $Q_T$ , were  
 308 computed using total cardiac flow as  $Q_T = Q_C \times Q_{TC}$  and  $Q_C = Q_{CC} \times BW^{0.75}$ .  $Q_{TC}$  values for the  
 309 percentages of cardiac flow to each tissue are given in Table 1. Finally, the drug concentration  
 310 entering tissues in the arterial blood is the free concentration of drug,  $C_{A,f}^i$ , and concentrations  
 311 leaving the tissues are calculated using the concentrations within the tissue compartment along  
 312 with the respective partition coefficients:  $C_{T,ven}^i = C_T^i / P_T$ .

313 Lung:

$$314 \quad \frac{dA_{lung}^i}{dt} = Q_C (C_{venous}^i - C_{L,ven}^i)$$

315 Kidney:

$$316 \quad \frac{dA_K^{RPT}}{dt} = Q_K \cdot (C_{A,f}^{RPT} - C_{K,ven}^{RPT}) - f_R \cdot CL^{RPT} \cdot C_{Art}^{RPT},$$

317 where  $CL$  and  $f_R$  are the total blood clearance and fractional renal clearance, respectively.

318 Liver and metabolism:

$$319 \quad v = \frac{V_M C_{liver}^{RPT}}{K_M + C_{liver}^{RPT} + \frac{(C_{liver}^{RPT})^2}{K_I}},$$

320      
$$\frac{dA_L^{RPT}}{dt} = Q_{LA} C_{A,f}^{RPT} + Q_S C_S^{RPT} + Q_G C_G^{RPT} - Q_L C_{L,ven}^{RPT} - (1-f_R) \cdot CL \cdot (Q_{LA} C_{A,rt}^i + Q_S C_S^i + Q_G C_G^i) / Q_L - v ,$$

321 where  $Q_L$  is the total blood flow leaving the liver and is the sum of the spleen, gut, and inlet liver  
 322 blood flow rates. Biliary clearance for RPT occurs in the liver where the fraction of total blood  
 323 clearance is equal to  $1 - f_R$ .

324    Gut:

325      
$$\frac{dA_G^{RPT}}{dt} = Q_G (C_{A,f}^{RPT} - C_{G,ven}^{RPT}) + k_{GLG} A_{GL}^{RPT} + k_{SG} A_{SG}^{RPT}$$

326

327    Stomach:

328      
$$\cdot \frac{dA_{Stom}^{RPT}}{dt} = F_a D \cdot d(t) - k_{SG} A_{Stom}^{RPT} ,$$

329 where  $F_a$  is the fractional absorption,  $D$  is the ingested dose, and  $d(t)$  describes the time  
 330 dependence of the dosing schedule.

331    Remaining tissues:

332      
$$\frac{dA_T^i}{dt} = Q_T (C_{A,f}^i - C_{T,ven}^i)$$

333    Arterial Blood:

334      
$$\frac{dA_A^i}{dt} = Q_C (C_{L,ven}^i - C_{A,f}^i) - \alpha^i f_R \cdot CL^{dRPT} \cdot C_{A,f}^{dRPT}$$

335 Renal clearance for dRPT occurs based on the free concentration of dRPT in the arterial blood  
 336 and is removed from the arterial blood compartment; therefore,  $\alpha^{RPT} = 0$  and  $\alpha^{dRPT} = 1$ .

337 Venous Blood:

$$338 \quad \frac{dA_V^i}{dt} = \sum_j^{N_r} Q_j C_{j,ven}^i + \beta^i v$$

339 All concentrations exiting the tissues are pooled in the venous blood compartment. Because there  
 340 is no liver compartment for the dRPT sub-model, any generation of dRPT is within the venous  
 341 blood; therefore,  $\beta^{RPT} = 0$  and  $\beta^{dRPT} = 1$ .

342 Peripheral Compartment:

$$343 \quad \frac{dA_P^{dRPT}}{dt} = Q_C (C_{A,f}^{dRPT} - C_{P,ven}^{dRPT}) - (1 - f_R) \cdot CL^{dRPT} \cdot C_{P,ven}^{dRPT}$$

344 Biliary clearance occurs within the peripheral compartment where the fraction of total clearance  
 345 is equal to  $1 - f_R$ .

346

## 347 REFERENCES

- 348 1. **Dooley KE, Savic RM, Park J-G, Cramer Y, Hafner R, Hogg E, Janik J, Marzinke MA, Patterson K, Benson CA, Hovind L, Dorman SE, Haas DW, ACTG A5311 Study Team.** 2015. Novel dosing strategies increase exposures of the potent antituberculosis drug rifapentine but are poorly tolerated in healthy volunteers. *Antimicrob Agents Chemother* **59**:3399–405.
- 353 2. **Zhang T, Zhang M, Rosenthal IM, Grosset JH, Nuermberger EL.** 2009. Short-course therapy with daily rifapentine in a murine model of latent tuberculosis infection. *Am J Respir Crit Care Med* **180**:1151–1158.
- 356 3. **Dooley KE, Bliven-Sizemore EE, Weiner M, Lu Y, Nuermberger EL, Hubbard WC, Fuchs EJ, Melia MT, Burman WJ, Dorman SE.** 2012. Safety and pharmacokinetics of escalating daily doses of the antituberculosis drug rifapentine in healthy volunteers. *Clin Pharmacol Ther* **91**:881–8.
- 360 4. **Savic RM, Lu Y, Bliven-Sizemore E, Weiner M, Nuermberger E, Burman W, Dorman SE, Dooley KE.** 2014. Population pharmacokinetics of rifapentine and desacetyl rifapentine in healthy volunteers: Nonlinearities in clearance and bioavailability. *Antimicrob Agents Chemother* **58**:3035–3042.
- 364 5. **Burman WJ, Gallicano K, Peloquin C.** 2001. Comparative pharmacokinetics and pharmacodynamics of the rifamycin antibiotics. *Clin Pharmacokinet* **40**:327–341.
- 366 6. **Munsiff SS, Kambili C, Ahuja SD.** 2006. Rifapentine for the treatment of pulmonary tuberculosis. *Clin Infect Dis* **43**:1468–1475.
- 368 7. **Rastogi N, Goh KS, Berchel M, Bryskier a.** 2000. Activity of rifapentine and its metabolite 25-O-desacetylrifapentine compared with rifampicin and rifabutin against *Mycobacterium tuberculosis*, *Mycobacterium africanum*, *Mycobacterium bovis* and *M. bovis* BCG. *J Antimicrob Chemother* **46**:565–570.
- 372 8. **Keung AC, Eller MG, Weir SJ.** 1998. Single-Dose Pharmacokinetics of Rifapentine in Women. *J Pharmacokinet Biopharm* **26**:75–85.
- 374 9. **Keung AC, Eller MG, Weir SJ.** 1998. Single-dose pharmacokinetics of rifapentine in elderly men. *Pharm Res* **15**:1286–1291.
- 376 10. **Keung AC, Eller MG, McKenzie KA, Weir SJ.** 1999. Single and multiple dose pharmacokinetics of rifapentine in man: Part II. *Int J Tuberc Lung Dis* **3**:437–444.
- 378 11. **Keung AC, Eller MG, Weir SJ.** 1998. Pharmacokinetics of rifapentine in patients with varying degrees of hepatic dysfunction. *J Clin Pharmacol* **38**:517–524.
- 380 12. **Langdon G, Wilkins JJ, Smith PJ, McIlleron H.** 2004. Consecutive-dose pharmacokinetics of rifapentine in patients diagnosed with pulmonary tuberculosis. *Int J Tuberc Lung Dis* **8**:862–867.
- 383 13. **Langdon G, Wilkins J, McFadyen L, Smith P, Simonsson USH, McIllemon H.** 2005. Population Pharmacokinetics of Rifapentine and Its Primary Desacetyl Metabolite in South African Tuberculosis Patients. *Population Pharmacokinetics of Rifapentine and Its Primary Desacetyl Metabolite in South African Tuberculosis Patients* **49**:4429–4436.

- Accepted Manuscript Posted Online  
Antimicrobial Agents and Chemotherapy  
AAC
- 387 14. **Weiner M, Bock N, Peloquin CA, Burman WJ, Khan A, Vernon A, Zhao Z, Weis S,**  
388 **Sterling TR, Hayden K, Goldberg S.** 2004. Pharmacokinetics of rifapentine at 600, 900,  
389 and 1,200 mg during once-weekly tuberculosis therapy. *Am J Respir Crit Care Med*  
390 **169:**1191–7.
- 391 15. **Reith K, Keung A, Toren PC, Cheng L, Eller MG, Weir SJ.** 1998. Disposition and  
392 metabolism of 14C-rifapentine in healthy volunteers. *Drug Metab Dispos* **26:**732–738.
- 393 16. **Dooley K, Flexner C, Hackman J, Peloquin CA, Nuermberger E, Chaisson RE,**  
394 **Dorman SE.** 2008. Repeated administration of high-dose intermittent rifapentine reduces  
395 rifapentine and moxifloxacin plasma concentrations. *Antimicrob Agents Chemother*  
396 **52:**4037–4042.
- 397 17. **Reisfeld B, Metzler CP, Lyons MA, Mayeno AN, Brooks EJ, DeGroote MA.** 2012. A  
398 Physiologically Based Pharmacokinetic Model for Capreomycin. *Antimicrob Agents  
399 Chemother*.
- 400 18. **Yue WY, Cohen SS.** 1966. Toxic nephritis with acute renal insufficiency caused by  
401 administration of capreomycin. Case report with necropsy findings. *Diseases of the chest*.
- 402 19. **Lyons M, Reisfeld B, Yang RSH, Lenaerts AJ.** 2013. A physiologically based  
403 pharmacokinetic model of rifampin in mice. *Antimicrob Agents Chemother* **57:**1763–71.
- 404 20. **Assandri A, Ratti B, Cristina T.** 1984. Pharmacokinetics of rifapentine, a new long  
405 lasting rifamycin, in the rat, the mouse and the rabbit. *J Antibiot (Tokyo)* **37:**1066–1075.
- 406 21. **Nakajima A, Fukami T, Kobayashi Y, Watanabe A, Nakajima M, Yokoi T.** 2011.  
407 Human arylacetamide deacetylase is responsible for deacetylation of rifamycins:  
408 Rifampicin, rifabutin, and rifapentine. *Biochem Pharmacol* **82:**1747–1756.
- 409 22. **Egelund EF, Weiner M, Singh RP, Prihoda TJ, Gelfond JAL, Derendorf H, Mac  
410 Kenzie WR, Peloquin CA.** 2014. Protein Binding of Rifapentine and Its 25-Desacetyl  
411 Metabolite in Patients with Pulmonary Tuberculosis. *Antimicrob Agents Chemother*  
412 **58:**4904–4910.
- 413 23. **Brown RP, Delp MD, Lindstedt SL, Rhomberg LR, Beliles RP.** 1997. Physiological  
414 parameter values for physiologically based pharmacokinetic models. *Toxicol Ind Health*  
415 **13:**407–84.
- 416 24. **Campbell JL, Clewell RA, Gentry PR, Andersen ME, Clewell HJ.** 2012.  
417 Physiologically based pharmacokinetic/toxicokinetic modeling. *Methods Mol Biol*  
418 **929:**439–99.
- 419 25. **Lumen A, McNally K, George N, Fisher JW, Loizou GD.** 2015. Quantitative global  
420 sensitivity analysis of a biologically based dose-response pregnancy model for the thyroid  
421 endocrine system. *Front Pharmacol* **6:**107.
- 422 26. **Chiu WA, Okino MS, Evans M V.** 2009. Characterizing uncertainty and population  
423 variability in the toxicokinetics of trichloroethylene and metabolites in mice, rats, and  
424 humans using an updated database, physiologically based pharmacokinetic (PBPK)  
425 model, and Bayesian approach. *Toxicol Appl Pharmacol* **241:**36–60.
- 426 27. **Zurlinden TJ, Reisfeld B.** 2015. Physiologically based modeling of the pharmacokinetics

- 427                   of acetaminophen and its major metabolites in humans using a Bayesian population  
428                   approach. *Eur J Drug Metab Pharmacokinet.*
- 429     28. **Zurlinden TJ, Heard K, Reisfeld B.** 2015. A novel approach for estimating ingested  
430                   dose associated with paracetamol overdose. *Br J Clin Pharmacol.*
- 431     29. **Bormann I.** DigitizeIt. Available at <http://www.digitizeit.de>.
- 432     30. **Bois FY.** 2009. GNU MCSim: Bayesian statistical inference for SBML-coded systems  
433                   biology models. *Bioinformatics* **25**:1453–4.
- 434     31. **Python Language Reference version 2. 7.** Python Software Foundation. Python  
435                   Language Reference, version 2.7.
- 436     32. **van der Walt S, Colbert SC, Varoquaux G.** 2011. The NumPy Array: A Structure for  
437                   Efficient Numerical Computation. *Comput Sci Eng* **13**:22–30.
- 438     33. **Jones E, Oliphant TE, Peterson P.** 2001. SciPy: Open source scientific tools for Python  
439                   <http://www.scipy.org/>.
- 440     34. **Hunter JD.** 2007. Matplotlib: A 2D Graphics Environment. *Comput Sci Eng* **9**:90–95.
- 441     35. **Global Alliance for TB Drug Development.** 2008. Handbook of Anti-Tuberculosis  
442                   Agents. *Tuberculosis* **88**:85–170.
- 443     36. 2000. Targeted tuberculin testing and treatment of latent tuberculosis infection. American  
444                   Thoracic Society. *MMWR Recomm Rep* **49**:1–51.
- 445     37. **Swaminathan S, Narendran G, Venkatesan P, Iliyas S, Santhanakrishnan R, Menon  
446                   PA, Padmapriyadarsini C, Ramachandran R, Chinnaiyan P, Suhadev M, Sakthivel  
447                   R, Narayanan PR.** 2010. Efficacy of a 6-month versus 9-month intermittent treatment  
448                   regimen in HIV-infected patients with tuberculosis: A randomized clinical trial. *Am J  
449                   Respir Crit Care Med* **181**:743–751.
- 450     38. **Blumberg HM, Burman WJ, Chaisson RE, Daley CL, Etkind SC, Friedman LN,  
451                   Fujiwara P, Grzemska M, Hopewell PC, Iseman MD, Jasmer RM, Koppaka V,  
452                   Menzies RI, O'Brien RJ, Reves RR, Reichman LB, Simone PM, Starke JR, Vernon  
453                   AA.** 2003. American Thoracic Society/Centers for Disease Control and  
454                   Prevention/Infectious Diseases Society of America: treatment of tuberculosis. *Am J  
455                   Respir Crit Care Med* **167**:603–662.
- 456     39. **Dorman SE, Savic RM, Goldberg S, Stout JE, Schluger N, Muzanyi G, Johnson JL,  
457                   Nahid P, Hecker EJ, Heilig CM, Bozeman L, Feng P-JI, Moro RN, MacKenzie W,  
458                   Dooley KE, Nuermberger EL, Vernon A, Weiner M, Tuberculosis Trials  
459                   Consortium.** 2015. Daily rifapentine for treatment of pulmonary tuberculosis. A  
460                   randomized, dose-ranging trial. *Am J Respir Crit Care Med* **191**:333–43.
- 461     40. **California Department of Public Health.** 2016. Fact Sheet: 12-dose Isoniazid  
462                   (INH)/Rifapentine regimen for latent TB infection treatment.
- 463     41. **Chang KC, Leung CC, Yew WW, Chan SL, Tam CM.** 2006. Dosing schedules of 6-  
464                   month regimens and relapse for pulmonary tuberculosis. *Am J Respir Crit Care Med*  
465                   **174**:1153–8.

- Accepted Manuscript Posted Online
- Antimicrobial Agents and Chemotherapy
- AAC
- 466 42. **Saukkonen JJ, Cohn DL, Jasmer RM, Schenker S, Jereb JA, Nolan CM, Peloquin  
467 CA, Gordin FM, Nunes D, Strader DB, Bernardo J, Venkataraman R, Sterling  
468 TR.** 2006. An Official ATS Statement: Hepatotoxicity of Antituberculosis Therapy. *Am J  
469 Respir Crit Care Med* **174**:935–952.
- 470 43. **Lyons M a., Lenaerts AJ.** 2015. Computational pharmacokinetics/pharmacodynamics of  
471 rifampin in a mouse tuberculosis infection model. *J Pharmacokinet Pharmacodyn* **42**:375–  
472 389.
- 473 44. **Pienaar E, Dartois V, Linderman JJ, Kirschner DE.** 2015. In silico evaluation and  
474 exploration of antibiotic tuberculosis treatment regimens. *BMC Syst Biol* **9**:79.
- 475

476 **FIGURE LEGENDS**477 **Fig. 1:** PBPK model structure

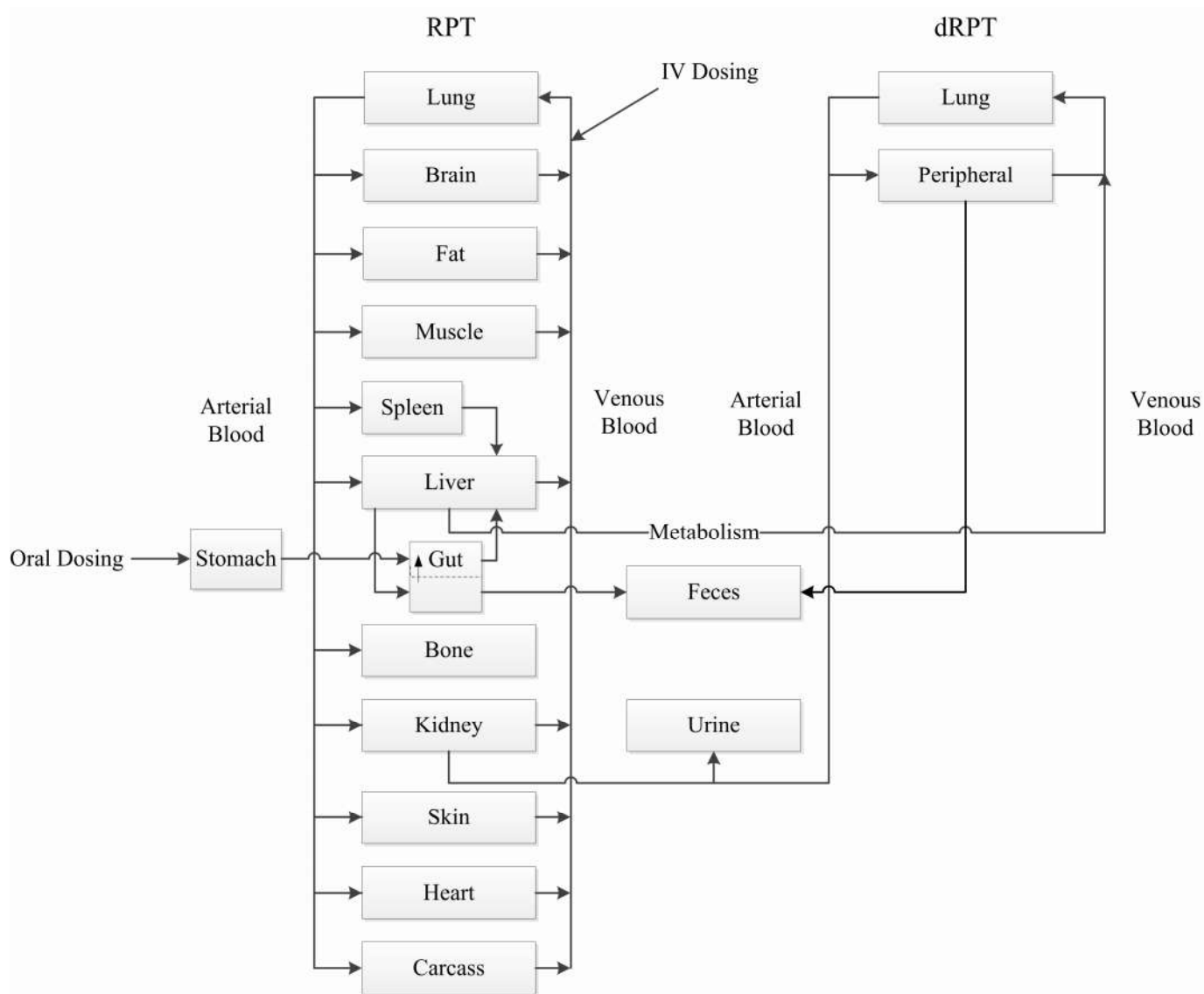
478 **Fig. 2:** Simulations of rifapentine pharmacokinetics following a 10 mg/kg oral dose in the rat, showing  
479 concentration profiles in the plasma (A), lung (B), kidney (C), and spleen (D). Solid and dashed lines  
480 represent the simulated mean and 95% prediction intervals, respectively; while transparent circles  
481 represent the training set data from Assandri et al. (20)

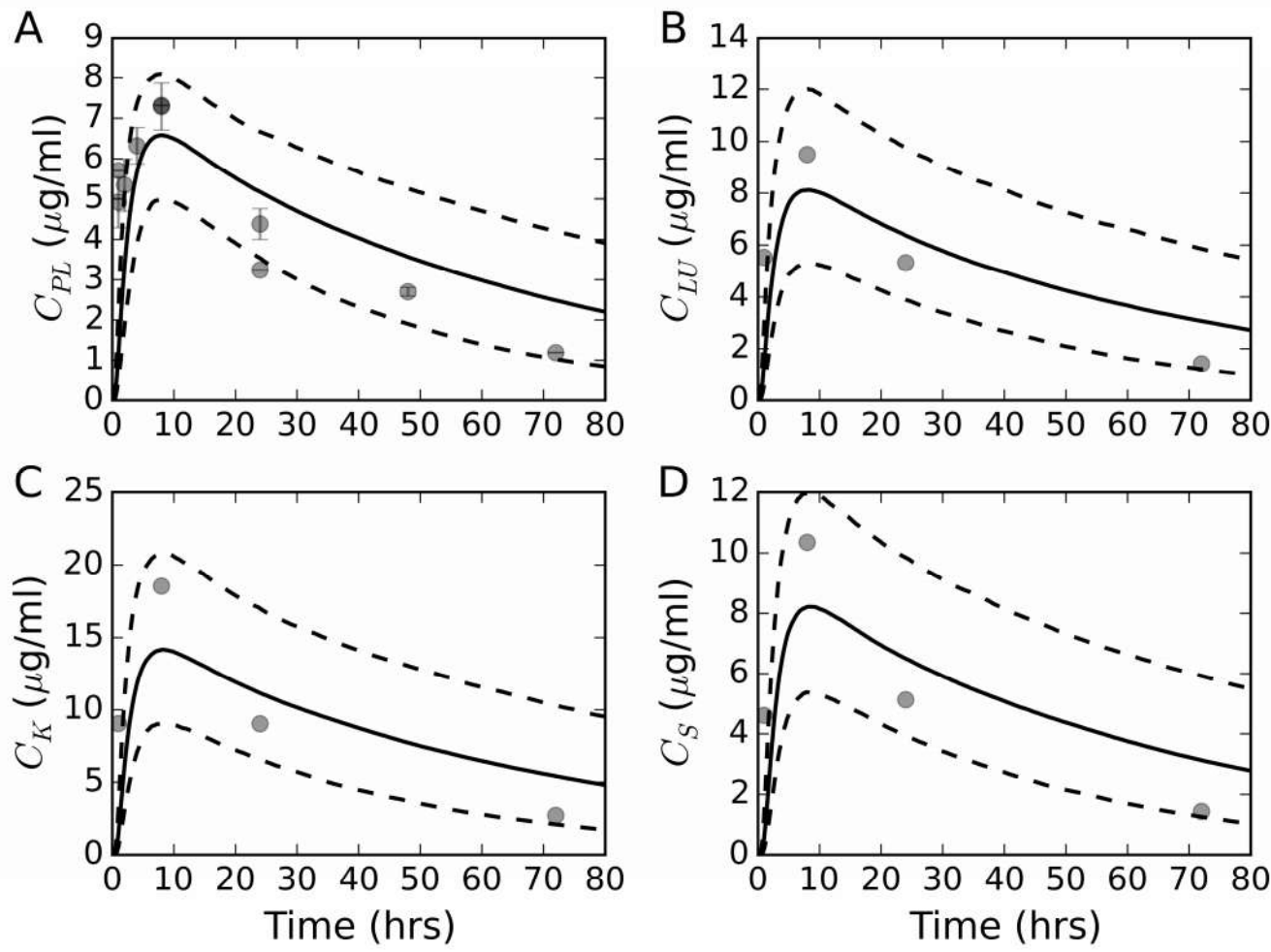
482 **Fig. 3:** Comparison of simulation results to human plasma concentration data for RPT and dRPT  
483 following oral administration of 600, 900, and 1200 mg oral RPT doses. Training set data are shown as  
484 transparent circles (o), while data from the validation set are shown as dark x's.

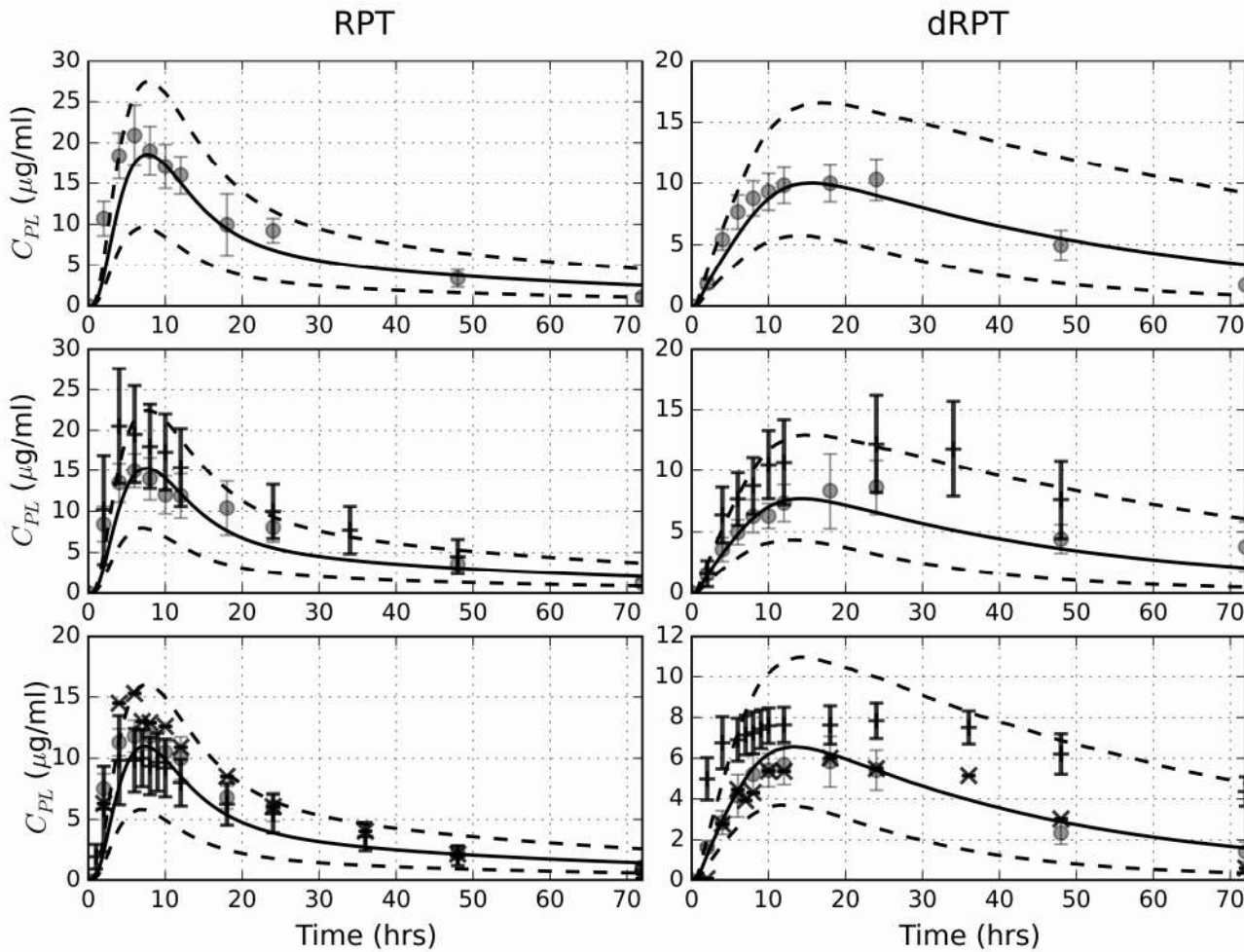
485 **Fig. 4:** Model verification for repeated dosing: predictions of plasma RPT concentrations for the three  
486 dosing regimens described in the text. Solid and dashed lines represent the simulated mean and 95%  
487 prediction intervals, respectively, while the triangles denote experimental data from the test set.

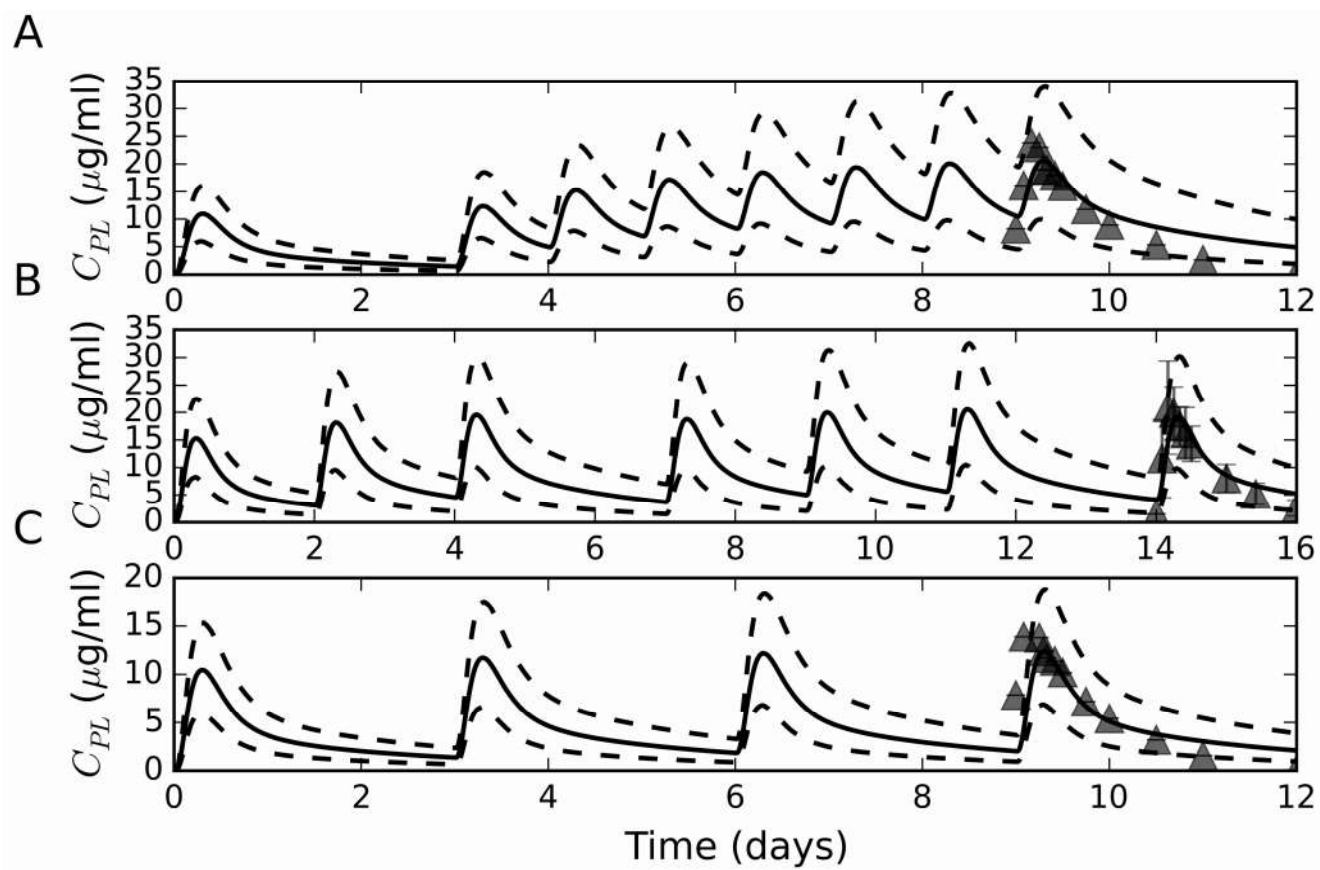
488 **Fig. 5:** Model predictions of time-course concentrations in the lung following the three repeated oral  
489 regimens described in Fig. 4, showing concentrations of RPT (solid line), dRPT (dashed line), and total  
490 rifamycin (dot-dashed line).

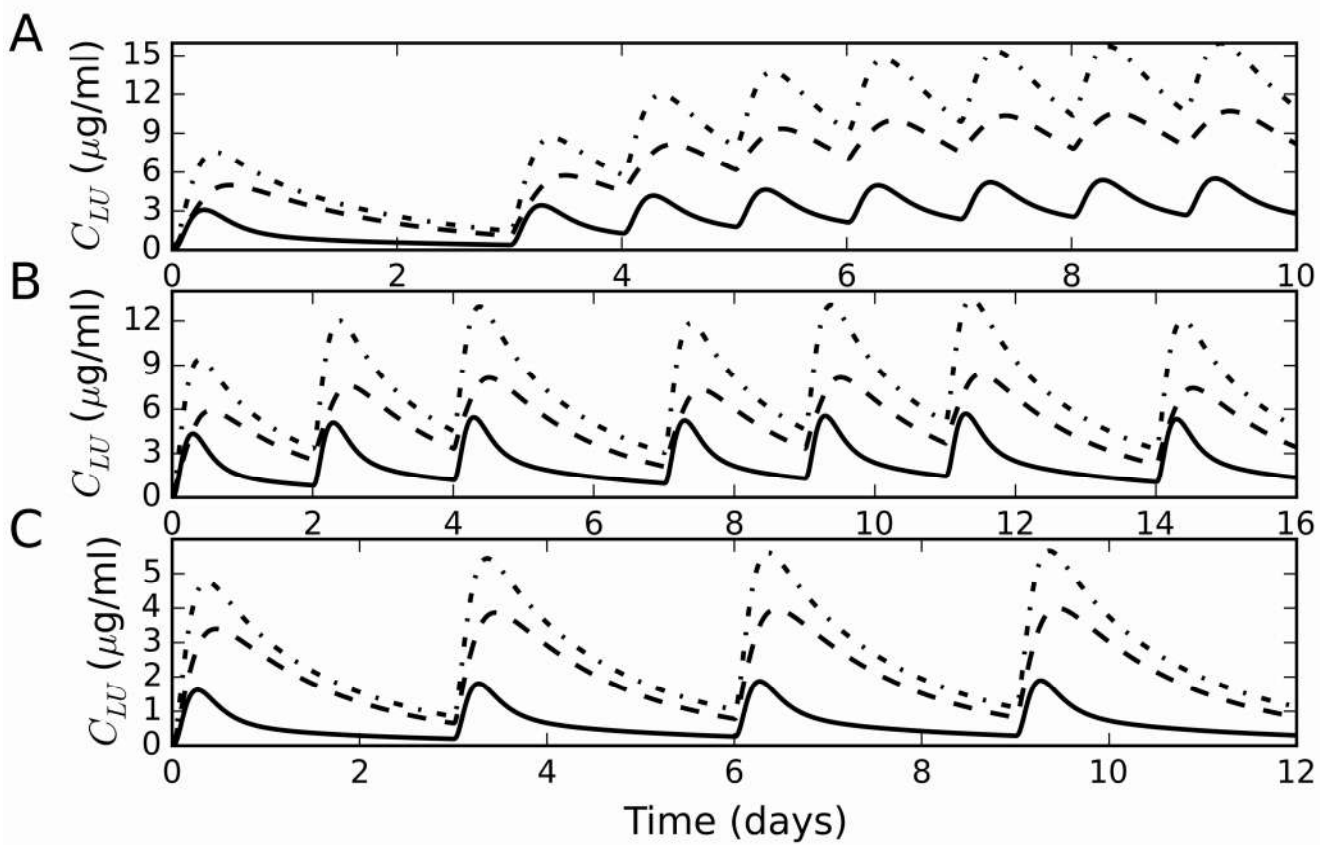
491 **Fig. 6:** Probability that the minimum steady-state concentration of RPT in the lung exceeds the minimum  
492 inhibitory concentration.











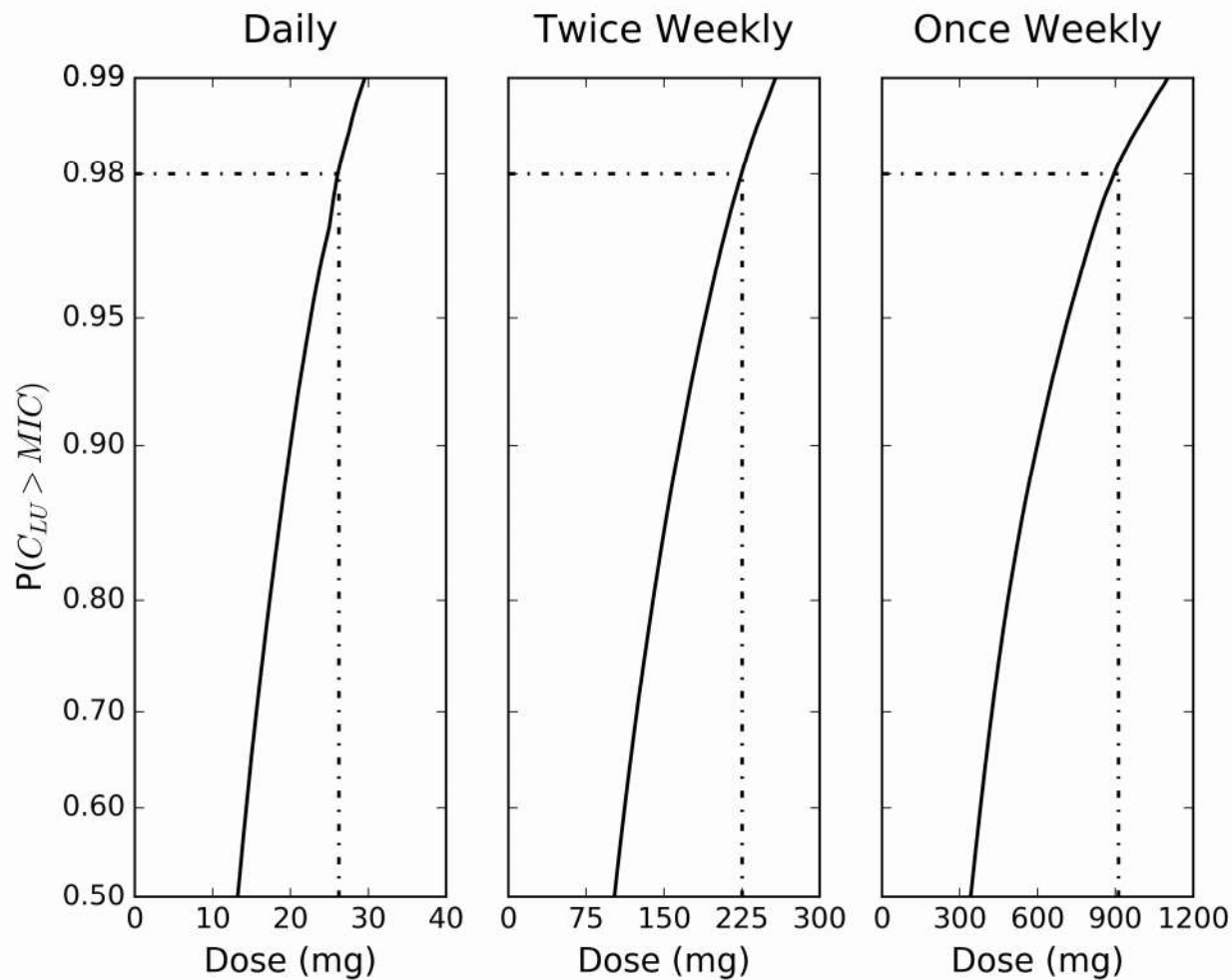


**Table 1: Physiological and anatomical parameters**

Parameter (units)	Abbreviation	Mean		Coefficient of Variation
		Rat	Human	
Body Weight (kg)	BW	0.23	65	0.16
Cardiac Output (L/h/kg <sup>0.75</sup> )	QCC	14.1	16.2	0.2
<b>Compartment</b>				
Lung	Q <sub>LUC</sub>	14.1	16.2	0.3
	V <sub>LUC</sub>	0.005	0.0076	0.2
Brain	Q <sub>BRC</sub>	0.02	0.12	0.3
	V <sub>BRC</sub>	0.0057	0.02	0.2
Fat	Q <sub>FC</sub>	0.07	0.0675	0.3
	V <sub>FC</sub>	0.07	0.2142	0.2
Heart	Q <sub>HC</sub>	0.049	0.045	0.3
	V <sub>HC</sub>	0.0033	0.0047	0.2
Muscle	Q <sub>MC</sub>	0.278	0.145	0.3
	V <sub>MC</sub>	0.4043	0.4	0.2
Bone	Q <sub>BC</sub>	0.122	0.05	0.3
	V <sub>BC</sub>	0.073	0.1429	0.2
Skin	Q <sub>SKC</sub>	0.058	0.05	0.3
	V <sub>SKC</sub>	0.1903	0.0371	0.2
Kidney	Q <sub>KC</sub>	0.141	0.18	0.3
	V <sub>KC</sub>	0.0073	0.0044	0.2
Spleen	Q <sub>SC</sub>	0.01	0.01	0.3
	V <sub>SC</sub>	0.002	0.0026	0.2
Gut	Q <sub>GC</sub>	0.14	0.14	0.3
	V <sub>GC</sub>	0.027	0.0171	0.2
Liver	Q <sub>LAC</sub>	0.024	0.06	0.3
	V <sub>LC</sub>	0.0366	0.0257	0.2
Carcass	Q <sub>CRC</sub>	0.088	0.1325	0.3
	V <sub>CRC</sub>	0.1015	0.0448	0.2
Venous Blood	V <sub>BLVC</sub>	0.0493	0.0526	0.2
Arterial Blood	V <sub>BLAC</sub>	0.0247	0.0263	0.2

**Table 2: Studies containing pharmacokinetic data for humans following oral dosing of rifapentine**

References	Dose	Regimen: single dose (S) or repeated dose (R)	TB Infected	Number of subjects (sex)
<b>Data used for parameter estimation</b>				
Weiner, 2004 (13)	1200 mg 900 mg 600 mg	R: once weekly	Yes	35 (M/F)
<b>Data used for model testing/verification</b>				
Dooley, 2008 (15)	900 mg	R: three times weekly	No	15 (M/F)
Dooley, 2012 (3)	1200 mg 900 mg 600 mg	S R: daily dosing	No	5 (M/F)
Keung, 1998 (10)	600 mg	S	No	20 (M/F)
Keung, 1998 (8)	600 mg	S	No	20 (M)
Keung, 1998 (7)	600 mg	S	No	15 (F)
Keung, 1999 (9)	600 mg 300 mg 150 mg	S R: daily dosing	No	23 (M)
Langdon 2004 (11)	600 mg 750 mg 900 mg	R: daily dosing, 4 days	Yes	46 (M/F)
Reith, 1998 (14)	600 mg	S	No	4 (M)

**Table 3: Physicochemical, biochemical, and clearance-related parameters**

Description	Parameter (units)	Rat			Human		
		Prior	Posterior	Source	Prior	Posterior	Source
<b>Fraction bound</b>							
RPT	$f_{b,R}$	-	0.97	(19)	-	0.994	(20)
dRPT	$f_{b,D}$	-	-	-	-	0.976	(20)
<b>Absorption</b>							
Fractional absorption constant	$F_{a,k}$	U(1, 1000)	N(27, 0.21)	-	N(27, 0.21)	N(21.23, 0.16)	Rat
Oral absorption rate	$k_{SG}$ (1/h)	N(0.31, 0.2)	N(0.30, 0.06)	(19)	N(0.30, 0.06)	N(0.33, 0.18)	Rat
Gut lumen reabsorption	$k_{GLG}$ (1/h)	N(0.17, 0.3)	N(0.17, 0.06)	(18)	N(0.17, 0.06)	N(0.17, 0.06)	Rat
<b>Total blood clearance</b>							
RPT	$CLC_R$ (L/h-BW <sup>0.75</sup> )	U(0.01, 10)	N(0.74, 0.31)	-	N(0.74, 0.31)	N(0.64, 0.18)	Rat
dRPT	$CLC_D$ (L/h-BW <sup>0.75</sup> )	-	-	-	U(0.001, 100)	N(0.07, 0.28)	-
Fractional renal clearance	$f_R$	-	0.13	(19)	-	0.13	Rat
<b>Deacetylation</b>							
	$V_{max}C$ ( $\mu\text{mol}/\text{h}\cdot\text{BW}^{0.75}$ )	-	-	-	U(0.01, 100)	N(0.97, 0.22)	(37)
	$K_M$ ( $\mu\text{mol}$ )	-	-	-	N(37.1, 0.2)	N(34.29, 0.16)	
	$K_I$ ( $\mu\text{mol}$ )	-	-	-	N(174, 0.2)	N(168.07, 0.17)	
<b>Partition Coefficients</b>							
Lung	$P_{LU}$	N(48.9, 0.2)	N(48.48, 0.17)	(19)	-	N(48.48, 0.17)	-
Brain	$P_{BR}$	N(5.93, 0.2)	N(5.81, 0.17)		-	N(5.81, 0.17)	
Fat	$P_F$	N(79.8, 0.2)	N(78.67, 0.17)		-	N(78.67, 0.17)	
Heart	$P_H$	N(63.9, 0.2)	N(62.02, 0.18)		-	N(62.02, 0.18)	
Muscle	$P_M$	N(38.1, 0.2)	N(37.39, 0.17)		-	N(37.39, 0.17)	
Bone	$P_B$	N(28.3, 0.2)	N(27.33, 0.18)		-	N(27.33, 0.18)	
Skin	$P_{SK}$	N(43.5, 0.2)	N(43.22, 0.17)		-	N(43.22, 0.17)	
Kidney	$P_K$	N(88.7, 0.2)	N(87.47, 0.17)		-	N(87.47, 0.17)	
Spleen	$P_S$	N(49.9, 0.2)	N(49.71, 0.17)		-	N(49.71, 0.17)	
Gut	$P_G$	N(42.1, 0.2)	N(38.69, 0.18)		-	N(38.69, 0.18)	
Liver	$P_L$	N(183.3, 0.2)	N(164.21, 0.18)		-	N(164.21, 0.18)	
Carcass	$P_{CR}$	N(28.3, 0.2)	N(29.04, 0.18)		-	N(29.04, 0.18)	
Peripheral	$P_P$	-	-		U(0.1, 200)	N(5.50, 0.29)	

$N(a, b)$  denotes a normal distribution with a mean of  $a$  and fractional coefficient of variation,  $b$ ;  $U(a, b)$  represents a uniform distribution bounded by the minimum ( $a$ ) and maximum ( $b$ ); a single number in the *posterior* column represents no distribution. When “Rat” is specified as the source, the posterior mean used in the R-PBPK (with a fractional CV of 0.3) was used as the prior distribution for the H-PBPK.

**Table 4: Computed pharmacokinetic measures for rifapentine**

Measures were derived from pharmacokinetic data (or simulation results) for a regimen consisting of a 900-mg dose administered repeatedly, four days apart. Shown are median properties (% CV)

<b>Parameter</b>	<b>Symbol (units)</b>	<b>Model Prediction</b>	<b>Experiment<sup>*</sup></b>
maximum plasma concentration	$C_{\max}$ ( $\mu\text{g}/\text{ml}$ )	15.48 (21)	15.48 (30)
drug half-life	$t_{1/2}$	10.92 (14)	12.03 (20)
area under the curve from time 0 extrapolated to infinity	$AUC_{0-\infty}$ ( $\mu\text{g}\cdot\text{h}/\text{ml}$ )	382.19 (25)	380.63 (31)
apparent oral clearance	CL/F (L/h)	1.69 (29)	1.92 (44)
apparent volume of distribution	V/F (L)	40.81 (29)	35.85 (47)

<sup>\*</sup>Observed values reported from ‘occasion 2’ of Langdon et al. (11)